Microscopic origin of thermal conductivity reduction in disordered van der Waals solids

Paul Erhart,*,† Per Hyldgaard,‡ and Daniel O. Lindroth†

Chalmers University of Technology, Department of Applied Physics, Gothenburg, Sweden , and Chalmers University of Technology, Department of Microtechnology and Nanoscience, Gothenburg, Sweden

E-mail: erhart@chalmers.se

Abstract

Films of layered substances like WSe_2 can exhibit a reduction in the out-of-plane thermal conductivity by more than one order of magnitude compared to the bulk, effectively beating the glass limit [Science **2007**, *315*, 351]. Here, we investigate the microscopic contributions that govern this behavior within the framework of Boltzmann transport theory informed by first-principles calculations. To quantitatively reproduce both the magnitude and the temperature dependence of the experimental data one must account for both phonon confinement effects (softening and localization) and interlayer scattering. Both stacking order and layer spacing are shown to have a pronounced effect on the thermal conductivity that could be exploited to tune the balance between electrical and thermal conductivity.

*To whom correspondence should be addressed

†Chalmers University of Technology, Department of Applied Physics, Gothenburg, Sweden

‡Chalmers University of Technology, Department of Microtechnology and Nanoscience, Gothenburg, Sweden

1 Introduction

The ability to manipulate the thermal conductivity is crucial in various contexts including refrigeration, heat insulation, thermoelectric energy recovery, as well as rapid heat dissipation. Nanostructuring is a very powerful tool for tuning thermal conductivity in particular for ultra-low thermal conductors[1–4] and thermoelectrics.[5–7]

Here we focus on one of these systems namely tungsten diselenide (WSe_2). It is a prototypical layered compound and a bulk crystalline example for a class of materials for which the phrase van der Waals (vdW) solid has been coined.[8] These materials are comprised of two-dimensional sheets with strong mixed covalent-ionic bonding character, which are coupled to each other by comparably weak vdW interactions[9,10] and can be engineered to form multilayers as well as heterostructures.[11–13]

As a result of the significant difference between intra and intersheet bonding characteristics vdW materials exhibit strong anisotropy in many properties including the thermal conductivity. The out-of-plane conductivity $\kappa_\perp$ of e.g., WSe_2, is already low for perfectly crystalline material at a level of $1.5\,\mathrm{W/m\,K}$ at room temperature.[1] Chiritescu *et al.* demonstrated that in films deposited at room temperature $\kappa_\perp$ can be further reduced by up to a factor of 30 compared to single crystalline material, yielding values considerably below the theoretical limit.[1,14,15] This dramatic reduction was attributed to the localization of lattice vibrations due to a randomization of the stacking order of WSe_2 sheets. In the present contribution we explore this finding within the framework of Boltzmann transport theory and first-principles calculations with the objective to discriminate the essential microscopic factors and quantify their respective contribution. Eventually, the goal is to identify pathways for generalizing the approach to other materials.

From here on, the paper is organized as follows: The next section, describes our methodological approach and summarizes computational details. In Sect. 3, the effect of structure on the out-of-plane thermal conductivity is investigated, specifically considering stacking sequence and homogeneous out-of-plane expansion. The changes in the phonon band structure

that underlie the structural sensitivity of the conductivity are analyzed in Sect. 4. Based on the data obtained in Sect. 3 a model is formulated in Sect. 5 that captures the experimentally observed increase in average and variance of the interlayer spacing as well as interlayer scattering. The final model is found to match the experimental data both in magnitude and temperature dependence, and provides the basis for a discussion of the importance of different microscopic mechanisms and their implications in Sect. 6.

2 Methodology

2.1 Calculation of thermal conductivity

We seek to resolve the microscopic factors that give rise to the drastic reduction in the out-of-plane thermal conductivity $\kappa_\perp$ observed experimentally. As WSe_2 has a rather larger band gap and the temperature range of interest is low, electronic contributions are negligible whence we focus our attention entirely on the phononic (lattice) contribution. To obtain the latter, we analyze $\kappa_\perp$ within the framework of semi-classical Boltzmann transport theory, which in the relaxation time approximation (RTA) yields the following expression for the thermal conductivity tensor,[16]

$$\kappa_{\alpha\beta} = \frac{1}{\Omega N_q} \sum_{i\boldsymbol{q}} v_{\alpha,i}(\boldsymbol{q}) v_{\beta,i}(\boldsymbol{q}) \tau_i(\boldsymbol{q}, T) c_i(\boldsymbol{q}, T). \tag{1}$$

where Ω is the unit cell volume, N_q is the number of $\boldsymbol{q}$-points in the summation, and $v_{\alpha,i}(\boldsymbol{q}) = \partial\omega_i/\partial q_\alpha$ is the group velocity of mode i along Cartesian direction α at point $\boldsymbol{q}$ of the Brillouin zone with ω_i being the mode frequency. Both phonon frequencies and group velocities can be derived from the second-order force constant matrix.[17] The mode specific heat capacity $c_i(\boldsymbol{q}, T)$ is given by

$$c_i(\boldsymbol{q}, T) = k_B \frac{x^2 \exp x}{(1 - \exp x)^2} \quad \text{with} \quad x = \frac{\hbar\omega_i(\boldsymbol{q})}{k_B T}. \tag{2}$$

The lifetime $\tau_i(\boldsymbol{q}, T)$ is limited by a number of scattering processes including e.g., phonon-phonon, isotope mass variation, and disorder. According to the most simple approximation, known as Matthiessen's rule, their respective contributions are inversely additive, i.e. $\tau_{tot}^{-1} = \sum_k \tau_k^{-1}$.

Calculation of phonon-phonon scattering rates requires knowledge of not only the second but also third-order force constants.[18,19] This contribution has been previously addressed using first-principles calculations for (ideal) bulk WSe_2.[20] The phonon-phonon scattering channel dominates only for relatively large single crystalline samples with a comparably low defect density. It is therefore of minor importance in the present work, which is concerned with the effect of structural defects and disorder on the thermal conductivity. For simplicity, we therefore assume a mode and $\boldsymbol{q}$-independent phonon-phonon scattering limited lifetime, which follows a simple temperature dependence, $\tau_{ph-ph} = \alpha T^{-b}$, motivated by analytic theory.[21] Specifically, we choose $b = 0.8$ and $\alpha = 27\,\mathrm{ps\,K}^b$, which reproduces the experimentally measured out-of-plane conductivity, see Sect. 3 and Fig. 1.[22]

In Sects. 3 and 4, we will focus on structural effects on group velocities and frequencies. We will return to the discussion of scattering channels, specifically in connection with structural defects, in Sect. 5.

2.2 Computational details

Phonon dispersion relations were analyzed using the PHONOPY package[23] based on force constants obtained from density functional theory (DFT) calculations. The latter were carried using the projector augmented wave method[24] as implemented in the Vienna ab-initio simulation package (VASP).[25] We employed a plane wave energy cutoff of 290 eV an sampled the Brillouin zone using Γ-centered $12 \times 12 \times 3$ k-point grids with respect to the primitive cell. The bulk of the force constant calculations were carried out using supercells comprising $2 \times 2 \times 2$ primitive unit cells. Convergence tests with systems composed of up to $6 \times 6 \times 3$ unit cells showed no significant changes in the phonon dispersion.

To assess the sensitivity of our results to the treatment of exchange-correlation effects we used both the local density approximation (LDA) and the van der Waals density functional (vdW-DF) method that captures non-local correlations.[9,26–28] Our non-empirical vdW-DF studies are based on the new consistent-exchange version (vdW-DF-cx)[29] as implemented in VASP.[30,31]

Table 1: Properties of tungsten diselenide from experiment (Refs. 32 and 33) and calculation. The 0 K data do *not* include zero-point vibrations. The in-plane and out-of-plane lattice constants a and c are given in Å. z_{Se} denotes the internal coordinate associated with Se. The elastic constants c_{33} and c_{44} are given in GPa, and the temperature T in Kelvin.

Method	T	a	c	z_{Se}	c_{33}	c_{44}
LDA	0	3.249	12.819	0.620	52.5	21.2
	300	3.250	12.832	0.620		
vdW-DF-cx	0	3.280	13.014	0.620	57.3	21.1
	300	3.282	13.061	0.621		
Experiment	300	3.282	12.96	0.6211	52.1	18.6

As shown in Table 1, both LDA and vdW-DF-cx yield good agreement with experimental data for bulk WSe_2 with respect to crystallographic parameters and elastic constants. Here, finite temperature effects were taken into account on the level of the quasi-harmonic approximation. Note, that the good agreement obtained with the LDA functional for bulk WSe_2 is fortuitous[9] as it is the result of error cancellation.[34,35] This problem becomes apparent under uniaxial expansion perpendicular to the layers as the LDA is incapable of reproducing the correct asymptotic behavior and thus cannot be expected to properly describe the materials response under these conditions. Unless noted otherwise, below we report results obtained using the vdW-DF-cx functional.

3 Out-of-plane conductivity and structure

3.1 Defect-free material

Figure 1 shows the calculated out-of-plane conductivity as a function of temperature for different conditions in comparison with experiment. It represents the key results of the present work and in the following sections, we will successively discuss the different data.

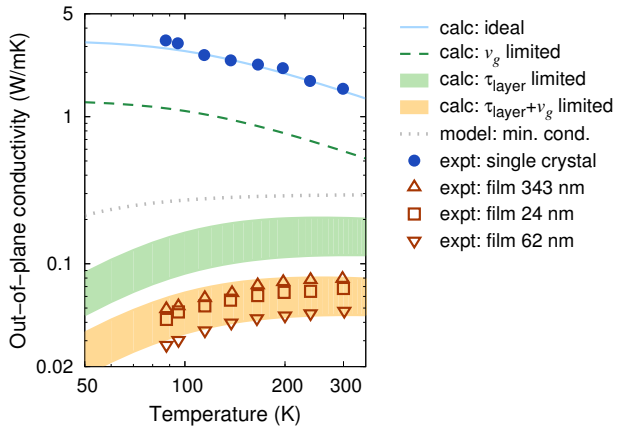

Figure 1: Out-of-plane lattice thermal conductivity $\kappa_\perp$ for various samples of WSe_2 from experiment (Ref. 1) and calculation. Blue circles and lines show the temperature dependence of $\kappa_\perp$ for ideal bulk material from experiment and calculation, respectively. Taking into account the effect of out-of-plane expansion and stacking disorder on the group velocities yields the $\kappa_\perp$ data shown by the dashed green curve (v_g limited). If only the effect of interlayer scattering on the lifetime is included one obtains the green data range (τ_{layer} limited), where the upper and lower limits correspond to $d = c = 13\,\text{Å}$ and $d = c/2 = 6.5\,\text{Å}$, respectively. To reach the experimental range of $\kappa_\perp$ obtained for disordered thin films (open red symbols), one must account for *both* group velocity reduction and interlayer scattering (yellow range, $\tau_{\text{layer}} + v_g$ limited). The minimal thermal conductivity that is predicted by the model introduced in Ref. 14 is shown by the dotted gray line.

The perfectly crystalline (ideal) system represents the starting point for the study of structural effects. As indicated above, in the present study we do not explicitly compute phonon-phonon scattering rates. Instead we use a simple lifetime model ($\tau_{\text{ph-ph}} = \alpha T^{-b}$) that is adjusted to reproduce the experimental single crystal data. The more important parameter is the prefactor α while the b parameter has only a minor effect and values approximately in the range 0.8 to 1.0 yield almost identical results.

3.2 Stacking disorder

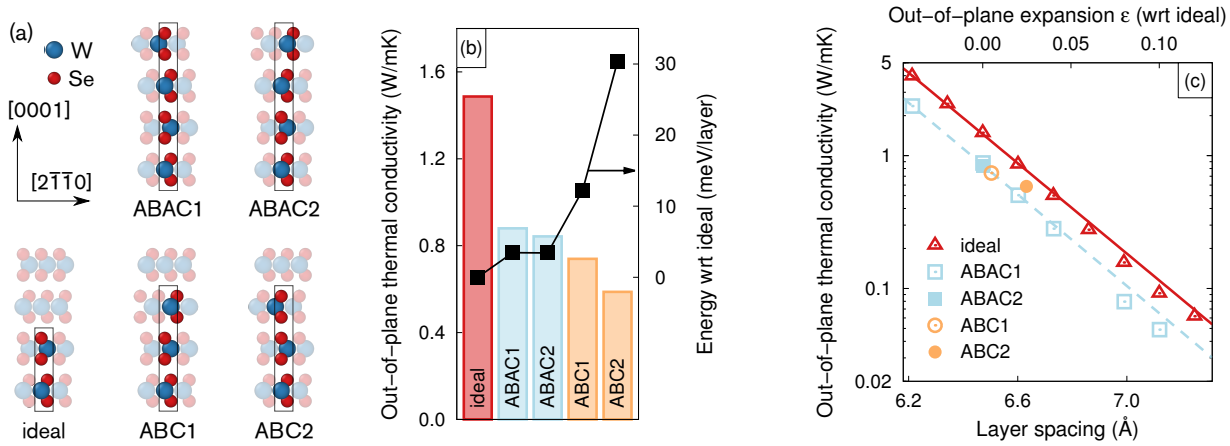

Figure 2: (a) Overview of the different types of stacking disorder considered in this study. The black boxes represent the respective unit cells. Out-of-plane thermal conductivity at 300 K (b) for the stacking disorder models shown in (a) and (c) as a function of layer spacing. The black solid curve in (b) shows the energy of the respective stacking sequence relative to the ideal structure. OVITO was used for structural analysis and visualization.[36]

To determine the impact of stacking disorder and layer separation on the out-of-plane conductivity $\kappa_\perp$, a number of different stacking faults were considered, which are illustrated in Fig. 2(a). They were obtained by altering the number and specific sequence of WSe_2 layers. In the equilibrium structure the W atoms occupy Wyckoff sites $2c$ and thus form a hexagonal closed packed[37] lattice with successive layers along [0001] labeled A and B, respectively. The Se atoms occupy Wyckoff sites $4f$ and form a sublattice, which follows the same stacking sequence as the W sublattice except that each layer comprises two Se atoms that have the same in-plane coordinate but are split along [0001]. In stacking sequence ABAC1 the W atoms follow an ABAC sequence while the Se atoms remain in ABAB sequence. Conversely in stacking sequence ABAC2 the Se atoms follow an ABAC pattern whereas the W atoms maintain the ABAB order. The ABC1 stacking fault configuration comprises Se and W atoms in ABC and ABB sequence, respectively, while in the ABC2 configuration the Se and W patterns are swapped. Each configuration was fully relaxed prior to the computation of the lattice thermal conductivity. For ABAC-type stacking, the calculations yield a very small energy increase relative to the ground state of only 3 meV/layer; slightly larger values

of 12 and 30 meV/layer are obtained for ABC1 and ABC2 stacking sequences.

Figure 2(b) shows the out-of-plane thermal conductivity that we have thus obtained for different stacking sequences. This reveals a reduction of $\kappa_\perp$ by 30 to 50%, which is still much less than the factor of 30 observed experimentally.[1] The effect of simple disorder in the stacking disorder is of similar magnitude for all configurations and thus does not exhibit a strong dependence on the number of affected layers. This can be expected since the interaction between neighboring layers is already weak whence long-range coupling should be even weaker. While our exploration of possible forms of stacking disorder is (computationally) limited it therefore appears unlikely that a reduction by more than an order of magnitude can be solely attributed to stacking disorder.

3.3 Interlayer separation

To proceed with our analysis it is relevant to revisit the information that is available from experiments concerning the structure and chemistry of turbostratically deposited thin films with ultralow thermal conductivity. The layer spacing obtained from X-ray diffraction is on average about 1.9–2.6% larger than the value for bulk WSe_2 (compare Table 1 and Refs. 1,2). Cross-sectional transmission electron micrographs[38] furthermore suggest a rather pronounced variation in layer separation.

As the first step in the analysis of these effects, Fig. 2(c) shows the variation of the out-of-plane conductivity $\kappa_\perp$ with layer separation, which reveals an exponential dependence with a reduction by a factor of 10 at 8% expansion. In these calculations the in-plane lattice constant was kept fixed at its zero-stress equilibrium value. The figure also contains equivalent data obtained for the ABAC1 stacking fault model as well as data for the other stacking sequences corresponding to their respective equilibrium layer spacing. Ideal and ABAC1 stacking exhibit a very similar dependence on layer spacing, suggesting that the stacking disorder and out-of-plane lattice expansion are not strongly coupled and can be considered additively. Furthermore, it is apparent that the variation among the non-ideal

stacking sequences can at least partially be rationalized in terms of variations in the layer spacing that result from full ionic relaxation.

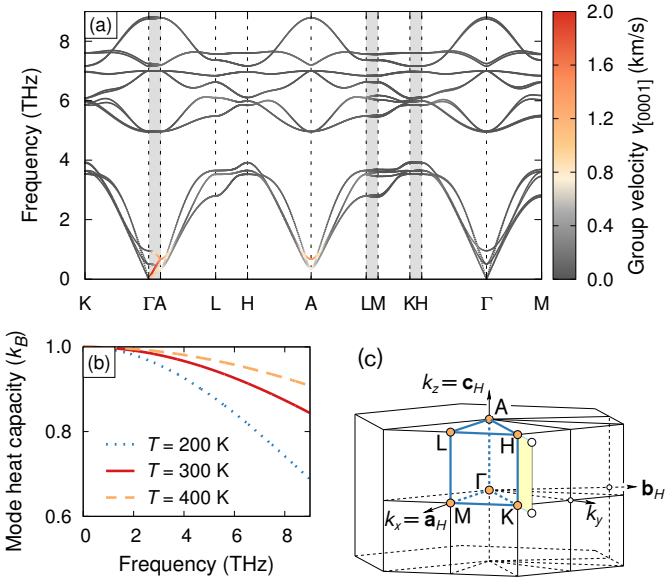

Figure 3: (a) Phonon dispersion relation for the fully relaxed equilibrium structure. The color scale indicates the group velocity along the z-direction for the respective mode. (b) Frequency dependence of the mode specific heat capacity. (c) Brillouin zone for space group $P6_3/mmc$ (International Tables of Crystallography no. 194, D^4_{6h}, Ref. 39).

4 Analysis of phonon dispersion relations

From our results it is apparent that even a moderate interlayer expansion produces a considerably larger reduction in the thermal conductivity than stacking disorder alone. As will be elaborated below, the exponential dependence of $\kappa_\perp$ on the layer spacing implies that one does not require a strong increase in the *average* layer spacing in order to achieve a dramatic reduction in $\kappa_\perp$ but merely *local variations* in layer spacings. We will return to this aspect in Sect. 5. First, we will address the microscopic mechanisms behind the reduction of $\kappa_\perp$ and compare the calculated vibrational properties with experiment, where possible.

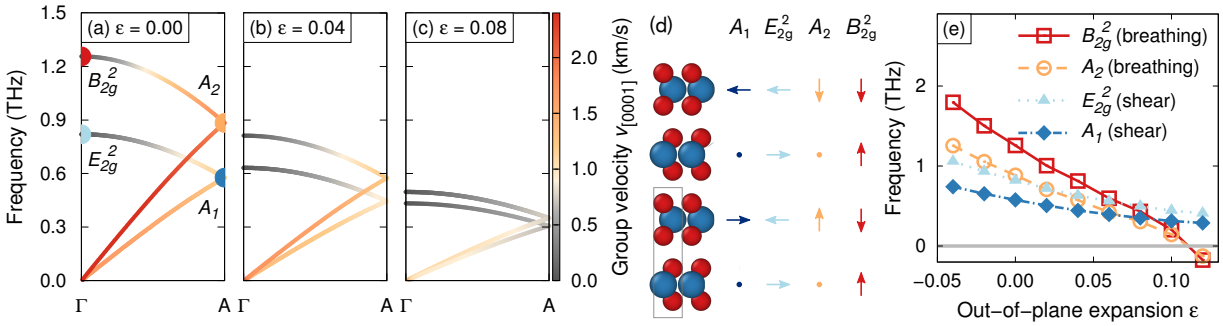

Figure 4: (a–c) Phonon dispersion along Γ-A for three different values of the out-of-plane expansion ε. The color scale indicates the group velocity along the z-direction. The colored circles in (a) indicate the zone-center and boundary modes, whose atomic displacement patterns (representing phonon polarization vectors) are shown in (d). These modes correspond to rigid shifts of layers with respect to each other as illustrated by the arrows. Panel (e) shows the dependence of the frequency of these modes on the out-of-plane expansion. The stability limit of the material with respect to out-of-plane expansion is determined by the breathing modes, whose frequencies become imaginary at approximately 11% when using vdW-DF-cx (7% for LDA).

4.1 Accordion effect

To resolve the microscopic origin for the $\kappa_\perp$ variation with layer separation, we analyzed the relative contributions of different phonon modes and $\boldsymbol{q}$-vectors to the summation in Eq. (1). Figure 3(a) shows the phonon dispersion for the fully relaxed structure. As we assume the relaxation time to be mode and $\boldsymbol{q}$ independent there are two terms that determine the contribution of any given mode to the thermal conductivity. The heat capacity $c_i(T, \boldsymbol{q})$ depends only on the frequency. As shown in Fig. 3(b), near room temperature this contribution is already close to saturation, i.e. $1\,k_B$ per mode, for all available frequencies.

The most important term is therefore the group velocity $v_{\alpha,j}(\boldsymbol{q})$ along [0001], which is indicated by the color scale in Fig. 3(a). It is obvious that only modes with $\boldsymbol{q}$-vector components along [0001] have non-zero $v_{\alpha,j}(\boldsymbol{q})$. The color-coding in Fig. 3(a) suggests that the dominant contributions to $\kappa_\perp$ stem from modes in the immediate vicinity of the Γ–A direction. A close-up of this branch is shown in Fig. 4 (a) at the equilibrium layer spacing as well as for out-of-plane expansions of (b) 4% and (c) 8%.

From Fig. 4(a) it is apparent that the main contribution to $\kappa_\perp$ at the equilibrium layer

separation stems from the longitudinal acoustic (LA) branch and, to a lesser extent, the lowest longitudinal optical (LO) mode. The atomic displacement patterns associated with these modes are shown in Fig. 4(d). With increasing layer separation the LA branch softens while the LO branch localizes leading to a considerable drop in the group velocity. This is further illustrated in Fig. 4(e), which shows the variation of the lowest energy zone-center and boundary modes with layer spacing. The A_2 breathing mode is a measure for the softness of the LA branch whereas the difference between the B^2_{2g} and A_2 breathing modes is associated with the localization of the lowest LO mode.

The stability limit of the material with respect to an expansion of the layer spacing is determined by the breathing modes, as they are the first modes to become unstable at about 11% expansion according to vdW-DF-cx (7% from LDA), see Fig. 4(e). This demonstrates that the material can tolerate a rather substantial level of expansion.

4.2 Comparison with experiment

The E^2_{2g} shear mode is Raman active and its frequency has been experimentally measured as 0.72 THz (24 cm^{-1}).[33] We obtain values of 0.82 THz (27 cm^{-1}) and 0.75 THz (25 cm^{-1}) from vdW-DF-cx and LDA calculations, respectively, where the latter value agrees with previous calculations.[33,40] Our calculations also agree well with experimental data for higher frequency Raman modes[41] as shown in Table 2

Table 2: Raman frequencies in cm^{-1} of bulk WSe_2 from experiment and calculation.

Mode	A_{1g}	E^1_{2g}	E_{1g}	E^2_{2g}
Experiment (Ref. 33)				24
Experiment (Ref. 41)	253	250	178	25
LDA	255	249	177	25
vdW-DF-cx	250	243	173	27

The longitudinal sound velocity along [0001] is determined by the group velocity in the long-wave limit, which gives about $c_{l,[0001]} = 2.0\,\mathrm{km/s}$ at the equilibrium layer spacing. This value is related to the elastic constant c_{33} via $c_{l,[0001]} = \sqrt{c_{33}/\rho}$, where ρ is the mass density.

The softening of the LA branch should therefore also be evident in the c_{33} elastic constant. In fact, while an experimental value of $c_{33} = 52\,\mathrm{GPa}$ has been obtained for bulk WSe_2,[33] a value of only 25 GPa was reported for WSe_2 with ultra-low thermal conductivity.[1,42] The observed (average) softening of the materials is thus approximately consistent with our calculations, which predict a reduction by one half for an expansion of about 3–4% for both vdW-DF-cx and LDA.

5 Microscopic model for $\kappa_\perp$ reduction

5.1 Variations in layer spacing

We are now in the position to provide a microscopic rationalization of the ultra-low thermal conductivity in WSe_2 films on the basis of our data. Recall that structural investigations of these films indicate that lower thermal conductivity is correlated with a decreasing coherence between crystallites in the films, a greater degree of misorientation,[2,38] an increase in the average layer spacing by 1.9–2.6% as well as a rather substantial variation in layer spacing along the out-of-plane direction.[43]

We first formulate a simple model to describe the average out-of-plane thermal conductivity $\kappa_\perp$ that results from a distribution in layer spacings. To approximate the experimental structure let us consider a stack of layers as schematically depicted in Fig. 5(a) with a distribution of layer spacings $l_1 = l_0(1+\varepsilon_i)$, where ε_i is the out-of-plane expansion relative to the ideal single crystal layer spacing l_0. The local thermal conductivity $\kappa(\varepsilon_i)$ reflects the expansion and $G_i = \kappa(\varepsilon_i)[l_0(1+\varepsilon_i)]^{-1}$ characterizes the thermal conductance across the "interface" between the i-th pair of layers.[44] In perfect single-crystalline WSe_2, the conductivity and intersheet conductance are $\kappa_0 = \kappa(0)$ and $G(0) = \kappa_0/l_0$, respectively.

As there is very limited information on the distribution of the intersheet spacings except for the average expansion[1] $\langle\varepsilon\rangle$, we simply assume an exponential distribution[45] $f(\varepsilon > 0) = \mu^{-1}\exp(-\varepsilon/\mu)$, where the mean of the distribution μ represents the average out-of-plane

expansion $\langle\varepsilon\rangle = \mu$. Figure 2(c) indicates an approximately exponential dependence of the out-of-plane conductivity on ε for the case of homogeneous expansion. We therefore set $\kappa(\varepsilon)/\kappa_0 = \exp(-a\varepsilon)$, where $a = 25.5$ gives a reasonable fit to our first-principles data.

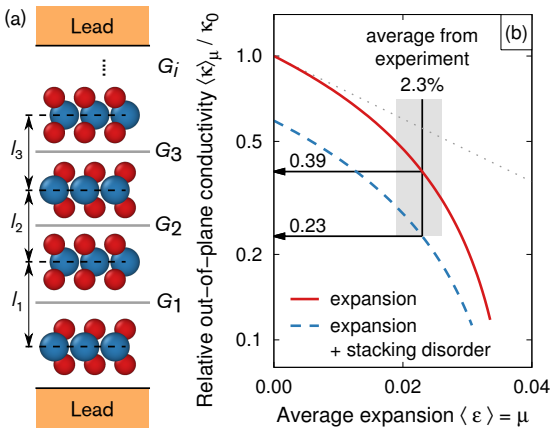

Figure 5: (a) One-dimensional model for a stack of WSe_2 layers with a distribution of layer spacings. The horizontal dashed lines indicate the "interfaces" between adjacent layers. (b) Effective out-of-plane conductivity across a stack with an exponential distributions of layer spacings as a function of the average out-of-plane expansion $\langle\varepsilon\rangle = \mu$. For reference, the exponential dependence of $\kappa_\perp$ obtained upon a *homogeneous* out-of-plane expansion, see Fig. 2(c), is represented by the dotted gray line. The gray bar represents the range of the experimentally observed average expansions (1.9–2.6%).

For a stack of N sheets the total thermal impedance is $G_N^{-1} = \sum_i G_i^{-1}$, where $Nl_0(1+\mu)G_N$ must approach the average effective thermal conductivity $\langle\kappa\rangle_\mu$ in the large-N limit. Replacing the N-stack thermal impedance by the distribution average[46]

$$\langle G^{-1}\rangle = \int d\varepsilon G^{-1}(\varepsilon) f(\varepsilon) / \int d\varepsilon f(\varepsilon), \tag{3}$$

we obtain $\langle\kappa\rangle/\kappa_0 = (\langle G^{-1}\rangle G(0))^{-1}(1+\mu)$. Discarding the last small factor $(1+\mu)$ but keeping the expansion effects in the ensemble averaging then yields the relative out-of-plane thermal conductivity as a function of the average expansion,

$$\frac{\langle\kappa\rangle_\mu}{\kappa_0} = \frac{1-a\mu}{1+\mu/(1-a\mu)}. \tag{4}$$

which is shown in Fig. 5(b).

For an average out-of-plane expansion of 2.3% representing the experimentally observed range of 1.9–2.6% that was discussed above, the model predicts a reduction of $\kappa_\perp$ by approximately 60% compared to the ideal structure. Stacking disorder causes a further reduction as indicated by the dashed blue curve in Fig. 5(b). It is because of the *variation* of layer spacings that the reduction predicted by the model is noticeably stronger than for the case of a pure homogeneous expansion, which is shown for comparison by the dotted gray line, also compare Fig. 2(c).

5.2 Lifetime limitation by interface scattering

Up to this point, the discussion has focused on structural effects on group velocities and frequencies. According to the analysis in the previous section, an increase in the average layer spacing along with local variations can explain a reduction of $\kappa_\perp$ by about 60%, also see Fig. 1 with stacking fault disorder having a slightly smaller effect. The temperature dependence of the "v_g limited" out-of-plane conductivity is indicated by the dashed green curve in Fig. 1. The thus obtained reduction is still noticeably above both the minimal conductivity model[14] and the values obtained for disordered WSe_2 films. This suggests that yet another mechanism is at work.

In fact, the perturbation of the periodicity perpendicular to the layers due to stacking faults and variations in layer spacing should not only affect the group velocities v_g but also limit the mean free path of phonon modes with out-of-plane components. This is equivalent to the effect of boundary scattering[17,47,48] and can be formally expressed in the form of another lifetime,[49]

$$\tau_{\text{layer}} = \frac{d}{v_{g,\perp}} \frac{1+p}{1-p}. \tag{5}$$

Here, $v_{g,\perp}$ is the projection of the group velocity on the out-of-plane direction, d represents

the upper limit on the phonon mean free path,[50] and p is a specularity parameter, which ranges from 0 for a completely rough edge to 1 for a perfectly smooth edge. In the case of a sample with perturbed periodicity and associated disorder, d should be comparable to the layer spacing, i.e., approximately between 6.5 and 13 Å. In fact, combining phonon-phonon scattering ($\tau_{\text{ph-ph}}$) and layer scattering (τ_{layer} with $p = 0$) with the group velocity limited thermal conductivity yields excellent agreement with the experimental data as shown by the yellow shaded region in Fig. 1 ($\tau_{\text{layer}} + v_g$ limited), where the lower (upper) limit corresponds to $d = 6.5$ Å (13 Å). Note that this calculation not only reproduces the experimental range for $\kappa_\perp$ at room temperature but, as a result of the temperature independence of τ_{layer}, also captures the experimental temperature dependence of $\kappa_\perp$, which primarily derives from the heat capacity, see Fig. 4(b).

It is important to point out that layer scattering alone *cannot* account for the experimental observations as demonstrated by the green shaded region (τ_{layer} limited). The latter can actually be considered the "glass limit" for the bulk material, in which the phonon mean free path is bound by the interatomic distance along the out-of-plane direction.

6 Discussion

The results and analysis presented in the previous sections allows us to provide a comprehensive description of the experimentally observed reduction of $\kappa_\perp$. The experimental characterization of WSe_2 films with ultralow thermal conductivity has revealed a pronounced degree of stacking disorder as well as an increase in not only the average layer spacing but also its variance. On a microscopic level the lattice thermal conductivity is determined by the group velocities v_g and lifetimes τ of the phonons in the material, see Eq. (1). A reduction of $\kappa_\perp$ can thus result from mode localization and softening (reducing v_g) as well as scattering (limiting τ).

The effects of stacking disorder and layer expansion on v_g were separately quantified in

Sect. 3. Stacking disorder causes a reduction of $\kappa_\perp$ due to localization and softening by 40–60%. While the homogeneous expansion of the out-of-plane separation gives rise to an exponential decrease of $\kappa_\perp$ it is not a realistic model for the structure of the material. The experimentally observed variation in layer spacing was therefore described in Sect. 5 using a simple analytic model for the distribution of layer spacings. Overall, the analysis suggests that *pure* phonon localization and softening ("phonon confinement", Refs. 51,52) can give rise to a reduction of $\kappa_\perp$ by a factor of 2 to 4, see Fig. 1.

The disorder in the WSe_2 films furthermore imposes a limit on the phonon mean free path in the out-of-plane direction, corresponding to an interface scattering limit on the lifetime τ. The minimum layer spacing in the out-of-plane direction (i.e., half the out-of-plane lattice constant, $d \approx c/2$ in Eq. (5)) in combination with a completely rough interface/boundary ($p = 0$) provides a lower bound for this scattering channel and effectively corresponds to the "glass limit".

To describe both the magnitude and the temperature dependence of the experimental $\kappa_\perp$, one must account for *both* the depression of group velocities and lifetimes assuming an effective interface spacing of only one to two lattice spacings (6.5–13.0 Å). Models that rely on phonon softening and localization only, are thus insufficient to describe the reduction of $\kappa_\perp$ in its entirety.[53]

The final value for $\kappa_\perp$ is naturally dependent on τ_{layer} as well as the effective reduction of $\kappa_\perp$, as indicated by the $\kappa_\perp$ range shown in Fig. 1. This merely reflects the fact that $\kappa_\perp$ is sensitive to small structural variations among different samples as evident from the experimental data.

It is interesting to note that the calculations presented in Sect. 3 demonstrate that a very significant reduction by 40–60% is possible by simply manipulating the stacking sequence. This effect can in principle be accomplished *without* introducing significant layer scattering (which is primarily the result of layer disorder). Given the small energy cost of ABAC-type stacking sequences and the recent advances in controlled deposition of vdW materials, this

possibility might be in fact realizable. Such an approach would be very interesting with respect to e.g., thermoelectric properties, for which one seeks to combine a relatively high electrical conductivity with minimal lattice thermal conductivities.[5] Electronic carriers typically have longer mean free paths than phonons and therefore should be less sensitive to the stacking order. Nanostructuring is of course well established in thermoelectric materials, primarily in the form of dopant, precipitate, and grain boundary engineering, see e.g., Ref. 7. Anisotropic structures offer additional and complementary possibilities as recently demonstrated for tilted multilayer structures.[54]

An even more significant reduction of $\kappa_\perp$ can be achieved by controlling the layer spacing. The latter could in principle be affected by strain, intercalation or more generally defect engineering. Further studies are in order to obtain a quantitative understanding of these mechanisms.

7 Conclusions

In summary, in this paper we have shown that the experimentally observed dramatic reduction of the out-of-plane thermal conductivity in disordered WSe_2 films can be quantitatively explained by a combination of Boltzmann transport theory and first-principles calculations. To explain the experimental result, one must account for the effect of disorder on both group velocities (phonon softening and localization) and lifetimes (scattering channels), as these mechanisms are individually insufficient to explain the experimental result. The results obtained here are of general relevance with respect to layered materials as the mechanisms described here are a result of variations in structure rather than chemistry. Finally, we note that controlling stacking disorder and layer spacing without scattering can be a powerful tool for manipulating phonon transport at least partly independently from charge-carrier transport. The latter ability is of interest in the context of e.g., thermoelectric materials and heat management.

Acknowledgments

We are thankful for helpful discussions with David C. Cahill (University of Illinois, Urbana-Champaign) and Andreas Klein (Technische Universität Darmstadt). This work has been supported by the Knut and Alice Wallenberg foundation, the "Area of Advance – Materials Science" at Chalmers, the Chalmers eScience center, and the Swedish foundation for strategic research. Computer time allocations by the Swedish National Infrastructure for Computing at NSC (Linköping) and C3SE (Gothenburg) are gratefully acknowledged.

Notes and References

(1) Chiritescu, C.; Cahill, D. G.; Nguyen, N.; Johnson, D.; Bodapati, A.; Keblinski, P.; Zschack, P. *Science* **2007**, *315*, 351–353.

(2) Nguyen, N. T.; Berseth, P. A.; Lin, Q.; Chiritescu, C.; Cahill, D. G.; Mavrokefalos, A.; Shi, L.; Zschack, P.; Anderson, M. D.; Anderson, I. M.; Johnson, D. C. *Chem. Mater.* **2010**, *22*, 2750–2756.

(3) Losego, M. D.; Grady, M. E.; Sottos, N. R.; Cahill, D. G.; Braun, P. V. *Nature Mater.* **2012**, *11*, 502–506.

(4) Ong, W.-L.; Rupich, S. M.; Talapin, D. V.; McGaughey, A. J. H.; Malen, J. A. *Nature Mater.* **2013**, *12*, 410–415.

(5) Snyder, G. J.; Toberer, E. S. *Nature Mater.* **2008**, *7*, 105–114.

(6) Heremans, J. P.; Jovovic, V.; Toberer, E. S.; Saramat, A.; Kurosaki, K.; Charoenphakdee, A.; Yamanaka, S.; Snyder, G. J. *Science* **2008**, *321*, 554–557.

(7) Biswas, K.; He, J.; Blum, I. D.; Wu, C.-I.; Hogan, T. P.; Seidman, D. N.; Dravid, V. P.; Kanatzidis, M. G. *Nature* **2012**, *489*, 414–418.

(8) Gao, G.; Gao, W.; Cannuccia, E.; Taha-Tijerina, J.; Balicas, L.; Mathkar, A.; Narayanan, T. N.; Liu, Z.; Gupta, B. K.; Peng, J.; Yin, Y.; Rubio, A.; Ajayan, P. M. *Nano Lett.* **2012**, *12*, 3518–3525.

(9) Rydberg, H.; Dion, M.; Jacobson, N.; Schröder, E.; Hyldgaard, P.; Simak, S. I.; Langreth, D. C.; Lundqvist, B. I. *Phys. Rev. Lett.* **2003**, *91*, 126402.

(10) Björkman, T.; Gulans, A.; Krasheninnikov, A. V.; Nieminen, R. M. *Phys. Rev. Lett.* **2012**, *108*, 235502.

(11) Cocemasov, A. I.; Nika, D. L.; Balandin, A. A. *Phys. Rev. B* **2013**, *88*, 035428.

(12) Chuang, S.; Kapadia, R.; Fang, H.; Chang, T. C.; Yen, W.-C.; Chueh, Y.-L.; Javey, A. *Appl. Phys. Lett.* **2013**, *102*, 242101.

(13) Geim, A. K.; Grigorieva, I. V. *Nature* **2013**, *499*, 419–425.

(14) Cahill, D. G.; Watson, S. K.; Pohl, R. O. *Phys. Rev. B* **1992**, *46*, 6131–6140.

(15) Chiritescu, C.; Cahill, D. G.; Heideman, C.; Lin, Q.; Mortensen, C.; Nguyen, N. T.; Johnson, D.; Rostek, R.; Böttner, H. *J. Appl. Phys.* **2008**, *104*, 033533.

(16) Berman, R. *Thermal Conduction in Solids*; Clarendon Press: Oxford, 1976.

(17) Ziman, J. M. *Electrons and phonons*; Clarendon Press: Oxford, 1960.

(18) Li, W.; Carrete, J.; Katcho, N. A.; Mingo, N. *Comp. Phys. Comm.* **2014**, *185*, 1747–1758.

(19) Li, W.; Carrete, J.; Mingo, N. *Appl. Phys. Lett.* **2013**, *103*, 253103.

(20) Kumar, S.; Schwingenschlögl, U. *Chem. Mater.* **2015**, *27*, 1278–1284.

(21) Slack, G. A. In *Solid State Physics*; Ehrenreich, F. S. H., Turnbull, D., Eds.; Academic Press, 1979; Vol. Volume 34; pp 1–71.

(22) The specific value of b is relatively unimportant as the analysis presented here is only very slightly affected as long as b is chosen from the range between approximately 0.7 and 1.1.

(23) Togo, A.; Oba, F.; Tanaka, I. *Phys. Rev. B* **2008**, *78*, 134106.

(24) (a) Blöchl, P. E. *Phys. Rev. B* **1994**, *50*, 17953 –17979; (b) Kresse, G.; Joubert, D. *Phys. Rev. B* **1999**, *59*, 1758 – 1775.

(25) (a) Kresse, G.; Hafner, J. *Phys. Rev. B* **1993**, *47*, 558–561; (b) Kresse, G.; Furthmüller, J. *Phys. Rev. B* **1996**, *54*, 11169.

(26) Dion, M.; Rydberg, H.; Schröder, E.; Langreth, D. C.; Lundqvist, B. I. *Phys. Rev. Lett.* **2004**, *92*, 246401.

(27) Thonhauser, T.; Cooper, V. R.; Li, S.; Puzder, A.; Hyldgaard, P.; Langreth, D. C. *Phys. Rev. B* **2007**, *76*, 125112.

(28) Berland, K.; Cooper, V. R.; Lee, K.; Schöder, E.; Thonhauser, T.; Hyldgaard, P.; Lundqvist, B. I. *Rep. Progr. Phys.* **2015**, *78*, 066501

(29) Berland, K.; Hyldgaard, P. *Phys. Rev. B* **2014**, *89*, 035412.

(30) Klimeš, J.; Bowler, D. R.; Michaelides, A. *Phys. Rev. B* **2011**, *83*, 195131.

(31) Björkman, T. *J. Chem. Phys.* **2014**, *141*, 074708.

(32) Schutte, W.; De Boer, J.; Jellinek, F. *J. Solid State Chem.* **1987**, *70*, 207–209.

(33) Zhao, Y.; Luo, X.; Li, H.; Zhang, J.; Araujo, P. T.; Gan, C. K.; Wu, J.; Zhang, H.; Quek, S. Y.; Dresselhaus, M. S.; Xiong, Q. *Nano Lett.* **2013**, *13*, 1007–1015.

(34) Murray, É. D.; Lee, K.; Langreth, D. C. *J. Chem. Theory Comput.* **2009**, *5*, 2754–2762.

(35) Berland, K.; Hyldgaard, P. *Phys. Rev. B* **2013**, *87*, 205421.

(36) Stukowski, A. *Model. Simul. Mater. Sci. Eng.* **2010**, *18*, 015012.

(37) Note that the W sublattice is hexagonal *close packed* only by name as the axial ratio is more than twice as large as the ideal ratio of $\sqrt{8/3}$.

(38) Kim, S.; Zuo, J. M.; Nguyen, N. T.; Johnson, D. C.; Cahill, D. G. *J. Mater. Res.* **2008**, *23*, 1064–1067.

(39) Tasci, E.; de la Flor, G.; Orobengoa, D.; Capillas, C.; Perez-Mato, J.; Aroyo, M. *EPJ Web of Conferences* **2012**, *22*, 00009.

(40) Ding, Y.; Wang, Y.; Ni, J.; Shi, L.; Shi, S.; Tang, W. *Physica B: Condensed Matter* **2011**, *406*, 2254–2260.

(41) Mead, D. G.; Irwin, J. C. *Canadian Journal of Physics* **1977**, *55*, 379–382.

(42) Note that in Ref. 1 the c_{33} value was actually derived from the longitudinal sound velocity, which was measured to be 1.65 km/s perpendicular to the film.

(43) See for example Fig. 3 in Ref. 38.

(44) Lee, S.-M.; Cahill, D. G.; Venkatasubramanian, R. *Appl. Phys. Lett.* **1997**, *70*, 2957.

(45) We have also considered Gaussian as well as truncated Gaussian distributions, where in the latter case the cutoff is given by the stability limit discussed in Sect. 4. These distributions lead to similar results as the exponential distribution and do not change the conclusions presented here. The exponential distribution has the advantage of involving only a single parameter, which can be fixed using experimental input, whereas the Gaussian distribution requires two parameters to be specified.

(46) The condition $a\mu < 1$ must be fulfilled in order for the integral in Eq. (3) to be convergent. Using the value of $a = 25.5$ calculated from first-principles one finds this condition implies $\mu < 0.04$, which is satisfied by the experimental value $\mu = \langle\varepsilon\rangle \approx 2.3\%$.

(47) Chen, G.; Tien, C. L.; Wu, X.; Smith, J. S. *Journal of Heat Transfer* **1994**, *116*, 325.

(48) Nika, D. L.; Pokatilov, E. P.; Askerov, A. S.; Balandin, A. A. *Phys. Rev. B* **2009**, *79*, 155413.

(49) Note that interface scattering has been discussed quite extensively in connection with the reduction of the thermal conductivity, in particular the *in-plane* component, in semiconductor superlattices, see e.g., Refs. 55,56.

(50) The boundary scattering model is commonly employed to describe the effect of finite sample size on phonon mediated thermal conduction, in which case d represents the

sample dimension. It effectively implements a geometric constraint on the mean free path of the individual phonon modes, i.e. $\lambda = v_g\tau \lesssim d$. It is in this more general context that the model is employed in the present work. For simplicity, we consider the limit $p = 0$, which corresponds to completely incoherent scattering. Any larger value of p (keeping all other parameters the same) would imply an increase in the thermal conductivity and thus an increasingly strong deviation from the experimental data. This in turn indicates that the layer scattering is in fact incoherent.

(51) Hyldgaard, P.; Mahan, G. D. *Phys. Rev. B* **1997**, *56*, 10754–10757.

(52) Balandin, A.; Wang, K. L. *Phys. Rev. B* **1998**, *58*, 1544–1549.

(53) Swartz, E. T.; Pohl, R. O. *Rev. Mod. Phys.* **1989**, *61*, 605–668.

(54) Sakai, A.; Kanno, T.; Takahashi, K.; Tamaki, H.; Kusada, H.; Yamada, Y.; Abe, H. *Sci. Rep.* **2014**, *4*.

(55) Chen, G. *Journal of Heat Transfer* **1997**, *119*, 220–229.

(56) Hyldgaard, P.; Mahan, G. D. Phonon Knudsen flow in GaAs/AlAs superlattices. Proceedings of the twenty-Third International Thermal Conductivity Conference. Lancaster, PA, 1996; p 172.

Table of Contents/Abstract graphic

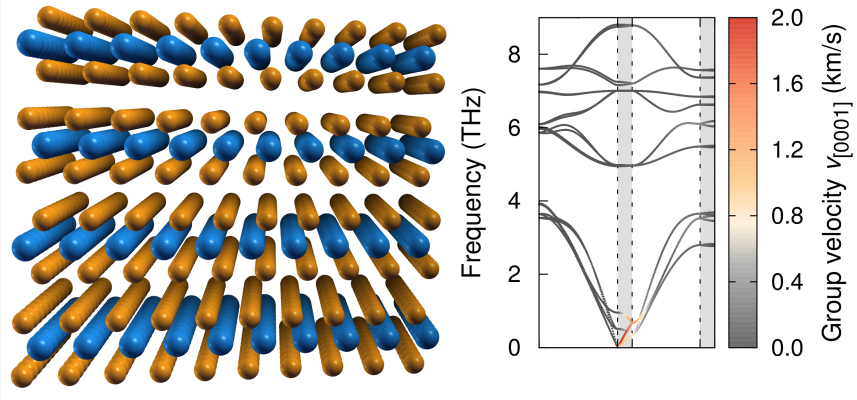

Layered compounds such as WSe_2 exhibit strongly anisotropic bonding, which gives rise to strong variations in phonon derived properties such as the thermal conductivity.